Numerical Simulation of Flow and Dispersion Around Buildings using CFD Model

Chan-Su Ryu

Department of Earth Science Chosun University, Kwangju 501-759, Korea

(Manuscript received on June 8, 2000)

A series of simulations were carried out to test the accuracy of a CFD (Computational Fluid Dynamics) model for flow and dispersion problems around buildings. The basic equations involved are Reynolds-averaged Navier-Stokes equations. Two different cases were selected to estimate the accuracy of a CFD model. Case 1 adopted Euler equations, which are obtained by neglecting the viscous fluxes from Reynolds-averaged Navier-Stokes equations, and Case 2 considered viscous fluxes, which can be closed by the $k-\varepsilon$ model for a turbulent close problem. The results of both cases were compared with wind tunnel data. The results for Case 2 were closer to the wind tunnel data than Case 1. Accordingly, this indicates that the inclusion of viscous fluxes in a CFD model is required for the simulation of flow and dispersion around buildings.

Key words : CFD, Dispersion, FEM

1. Introduction

The consequences of major accidents at military and industrial installations are increasingly being analysed using complex modeling techniques. A prime example of which relates to the near-field dispersion of toxic and hazardous gas in the immediate vicinity of buildings(project EMU)[1]. Flow and dispersion around buildings has been investigated for many years, particularly in the field of wind engineering and pollution. Very detailed descriptions of flow behavior around bluff bodies[2] were developed during the 80's based on experimental results. In many cases the descriptions were completely qualitative with mathematical relations between the problem variables such as the average wind inflow, characteristic measurements of the obstacle(length, width and height), density(ρ), roughness(z_0), etc.

However, the development of supercomputers has brought the possibility of treating such problems from a completely different perspective as a complement to the old experimental procedures. The first steps taken in this direction were related to solving the governing equations for problems where reasonable 2-D approximations

were possible, for example street canyons[3]. Yet, the long-term trend is moving toward full 3-D simulations[4,5]. Three-dimensional CFD(Computational Fluid Dynamics) techniques offer the capability to simulate realistic problems over complex obstacles such as topography and buildings. Although the safety-related applications of a CFD model related to dispersion are increasing, the validity of such predictions is still unconfirmed.

Accordingly, this study focused on testing the accuracy of CFD for two cases. Case 1 adopted Euler equations, which are obtained by neglecting the viscous fluxes from Reynolds-averaged Navier-Stokes equations, whereas Case 21 considered the viscous fluxes, which can be closed by the $k-\varepsilon$ model for a turbulent close problem. The results of both cases were compared with wind-tunnel data. Section 2 outlines the general procedure used when running a CFD code for specific simulations. The description of the problem and the model equations used in this study are given in sections 3 and 4, respectively. Section 5 presents the model output. A comparison between the model output and wind-tunnel data is given section 6. Finally, the conclusion and outlook are given in section 7.

2. Set-up Steps

For the simulation of any problem using a CFD model, a series of steps are required in order to arrive at the final result. An outline of the complete process is shown in diagram 1. The following is a brief summary of these steps.
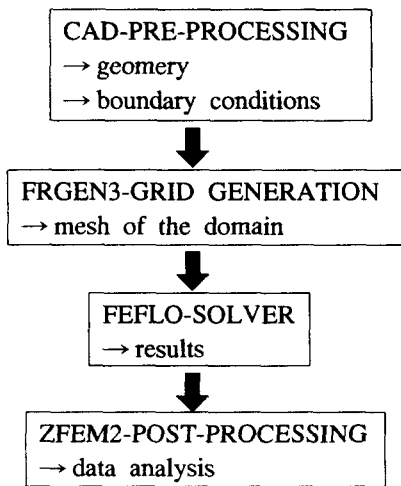
```
┌─────────────────────────────┐
│ CAD-PRE-PROCESSING          │
│ → geomery                   │
│ → boundary conditions       │
└─────────────────────────────┘
              │
              ▼
┌─────────────────────────────┐
│ FRGEN3-GRID GENERATION      │
│ → mesh of the domain        │
└─────────────────────────────┘
              │
              ▼
┌─────────────────────────────┐
│ FEFLO-SOLVER                │
│ → results                   │
└─────────────────────────────┘
              │
              ▼
┌─────────────────────────────┐
│ ZFEM2-POST-PROCESSING       │
│ → data analysis             │
└─────────────────────────────┘
```

Diagram 1. Steps for CFD run.

Step I : Geometric definition of the problem, known as pre-processing. For this part a CAD tool is used to input the geometry and boundary conditions of the problem.

Step II : Generation of a grid that covers the computational domain. Unstructured meshes using the advancing front methodology[6~9] were used in this study. As a result, any complex geometry can be automatically generated. The CAD file produced in the previous step is used as the input for this step.

Step III : Given a mesh, it is then possible to proceed to the solver step. In order to solve the problem a CFD code is used[10]. CFD can solve both compressible and incompressible fluid problems, either coupled to a structure or not. The output of this step is a numeric result.

Step VI : The last step is to analyse the data obtained by the solver, called post-processing. Since it is sometimes hard and tedious to gain a conclusion from the huge amount of data produced, a visualization tool is often helpful in the analysis[11~13].

3. Problem Description

The geometry in this study was an L-shaped building, the surface mesh close to the building is shown in Figure 1a. The boundary conditions applied to the problem were a fixed velocity and temperature in the inflow plane, characteristic in/outflow conditions in the outflow plane, a top plane for the computational domain, lateral planes that were parallel to the direction of the incoming flow, and a normal velocity equal to zero ($\vec{v} \cdot \hat{n} \mid_{surface} = 0$) on the bottom surface and the surfaces of the building. A non-uniform mesh was generated in order to produce a better flow field resolution in the areas of most interest, for example near the building. The mesh had 365,000 points and 2,030,000 tetrahedra. The general approach was to maximize the mesh density(and minimize mesh spacing) in regions where high gradients in the flow variables could be expected, yet without allowing the mesh expansion ratios to exceed about 1.2, since higher values can lead to significant errors. The obvious critical regions were those surrounding the sharp leading edges of the building and the near-source regions. Turbulence closure calculations of separated flows around blunt obstacles have demonstrated the need for a very fine resolution in regions where separation is expected. With regard to the spatial discretisation scheme used for the convective terms, the CFD code contained a number of options ranging from upwind differencing to self-filtered central differencing.

The source of the continuous release was from a door in the side of the building. The area of the door was 20 m^2 and the release rate was $Q_s = 20 \ m^3 \ s^{-1}$ in the normal door direction. The height of the building was $H = 10 \ m$. Figure 1b shows an aerial cross section of Fig. 1a. The vertical profile of the incoming wind was set to a logarithmic profile in the inflow plane:

$$U = \frac{u^*}{k} \ln\left(\frac{z}{z_0}\right) \qquad (1)$$

where u^* is the friction velocity($u^* = 0.0909 U_h$), k is the von Karman constant($k = 0.41$), and z_0 is the roughness length $z_0 = 0.12 m$[1]. The same case was also modelled in a wind tunnel. The mean

concentration data were extracted at a series of downwind points(the 'sensor positions'). These data were used for a comparison between the two cases.
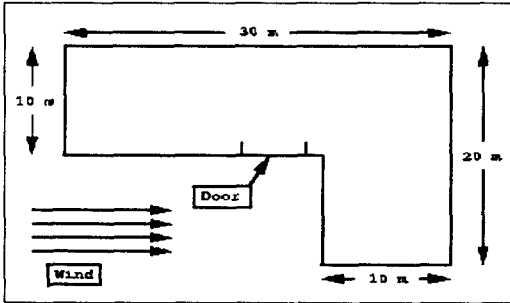
(a)
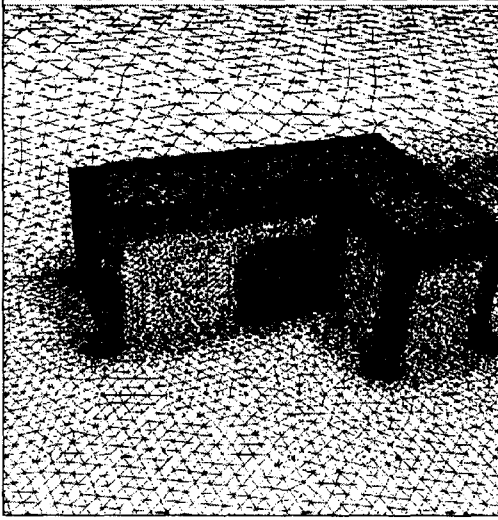
(b)

Fig. 1. (a) L-Shaped Building Mesh, (b) Top view of L-shape Building.

4. Model Equations

A three-dimensional CFD code based on the finite element technique was used to simulate the airflow and dispersion around the building. The model equations for the momentum and concentration are as follows.

$$\frac{\partial \overline{u_i}}{\partial t} + \frac{\partial}{\partial x_j}(\overline{u_i u_j}) = \qquad (2)$$
$$-\frac{1}{\rho}\frac{\partial \overline{p}}{\partial x_i} + \frac{\partial}{\partial x_j}(\overline{\tau_{ij}} - \overline{u_i' u_j'}) ,$$

$$\frac{\partial}{\partial x_k}(\overline{u_k}\ \overline{C}) = \frac{\partial}{\partial x_k}[(D+\eta)\frac{\partial \overline{C}}{\partial x_k}] , \qquad (3)$$

where,

$$\overline{\tau_{ij}} = \nu\ (\frac{\partial \overline{u_i}}{\partial x_j} + \frac{\partial \overline{u_j}}{\partial x_i}) . \qquad (4)$$

The bar and the prime denote the mean and the instantaneous values of the flow variables, respectively. The velocity, pressure, density, and concentration are represented by u, p, ρ, and C, respectively, plus ν is the molecular viscosity. D and η are the turbulent and molecular diffusivities, respectively.

To get a closed set of equations, it is necessary to relate the Reynolds stresses to other independent or dependent variables so as to complete the problem from a mathematical point of view. This is called the closure problem of turbulent flows. The most general approach in turbulence modeling is the use of the Boussinesq assumption which suggests that turbulent shear stresses are related to the rate of the mean strain through a turbulent eddy viscosity. For the general Reynolds stress tensor the Boussinesq assumption gives,

$$- \overline{u_i' u_j'} = \nu_t\ (\frac{\partial \overline{u_i}}{\partial x_j} + \frac{\partial \overline{u_j}}{\partial x_i}) - \frac{2}{3} k\delta_{ij} . \qquad (5)$$

where ν_t represents the eddy viscosity, k the turbulent kinetic energy, and δ_{ij} the Kronecker delta. In the $k-\varepsilon$ turbulence model, the viscosity ν_t and eddy mass diffusivity D are modeled as,

$$\nu_t = c_\mu \frac{k^2}{\varepsilon} , \qquad (6)$$

$$D = \frac{\nu_t}{\sigma_t} , \qquad (7)$$

respectively, where the constant c_μ is determined as 0.09 and ε is the dissipation rate of the turbulent kinetic energy. The value of the Schmidt number σ_t is assumed to be equal to the turbulent Prandtl number $\mathrm{Pr}_t = 0.8 \char`\~ 1.3$. The following modeled transport equations for k and ε are used.

$$\frac{\partial k}{\partial t} + \overline{u_i}\frac{\partial k}{\partial x_i} = \frac{\partial}{\partial x_i}(\frac{\nu_t}{\sigma_k}\frac{\partial k}{\partial x_i}) + P - \varepsilon , \qquad (8)$$

$$\frac{\partial \varepsilon}{\partial t} + \overline{u_i}\frac{\partial \varepsilon}{\partial x_i} = \frac{\partial}{\partial x_i}(\frac{\nu_t}{\sigma_\varepsilon}\frac{\partial \varepsilon}{\partial x_i}) + c_1\frac{\varepsilon}{k}P - c_2\frac{\varepsilon^2}{k} , \qquad (9)$$

$$P = \nu_t(\frac{\partial \overline{u_i}}{\partial x_j} + \frac{\partial \overline{u_j}}{\partial x_i})\frac{\partial \overline{u_i}}{\partial x_j} . \qquad (10)$$

where P is the production term, and σ_k, σ_ε, c_1, and c_2 are empirical constants with values of 1.0, 1.3, 1.44, and 1.92, respectively.

5. Results

This section presents the qualitative results for the flow field. All the plots were made with *zfem2* [11].

5.1 Simulated Flow field around Buildings

Figure 2 shows the contour of the absolute value of the velocity in a plane perpendicular to the x direction that was in the main flow direction. Figures 2a and 2b represent cases 1 and 2, respectively. Figure 2a clearly shows a separation due to the bluff corner of the building. The separation and re-attachment followed patterns as discussed in previous literature[2]. Figure 2b using the $k-\varepsilon$ model shows more or less the same trend as in case 1. The contour of the velocity depicted recirculation on the roof with re-attachement. The maximum velocities of cases 1 and 2 were 5.85 $m\ s^{-1}$ and 5.53 $m\ s^{-1}$, respectively. Case I exhibited two clear circulation cells on the roof, whereas case 2 only had one.
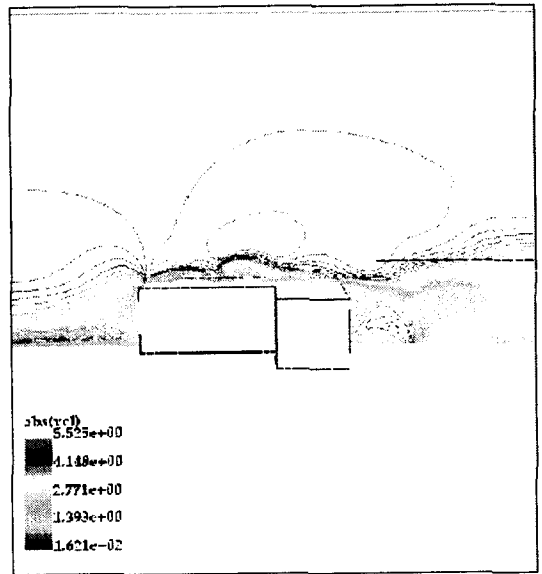
(a)
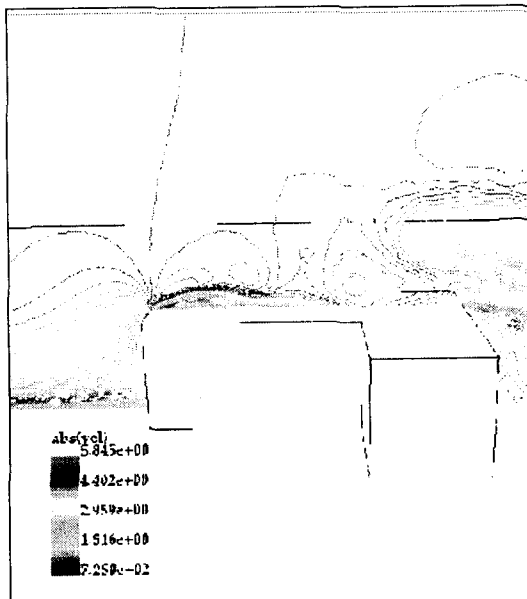
(b)

Fig. 2. Contours of velocity for (a) Case 1 and (b) Case 2.

Figure 3 shows the wind vector for both cases. Recirculation was observed at the upwind wall of the building in both cases. As Hosker[2] remarked, case I has a relatively bigger vortex in front of the obstacle than case 2. It should be emphasized that if the incoming flow is uniform, recirculation will not exist[2]. There was also a stagnation point half-way up the building in both cases.

5.2 Simulated Concentration around Buildings

The isosurface with a 10 % concentration is shown in Fig. 4 for both cases. The cloud shown in Figure 4a was not so diffuse because the turbulence process was not considered in this model, however, the cloud shown in Fig. 4b was more diffused at the back and at both sides of the building. The color scale on top of both clouds indicates the velocity at those points. The maximum concentrations were 6.0 and 5.67 for case 1 and 2, respectively. Case 2 exhibited more turbulence related to the concentration dispersion around the building. This was because case 2 included viscous fluxes which were not considered in case 1.

Figures 5, 6, and 7 show the flow currents for both cases using ribbons colored by the wind velocity at the surface level(0.2 m), 5m, and 8m,
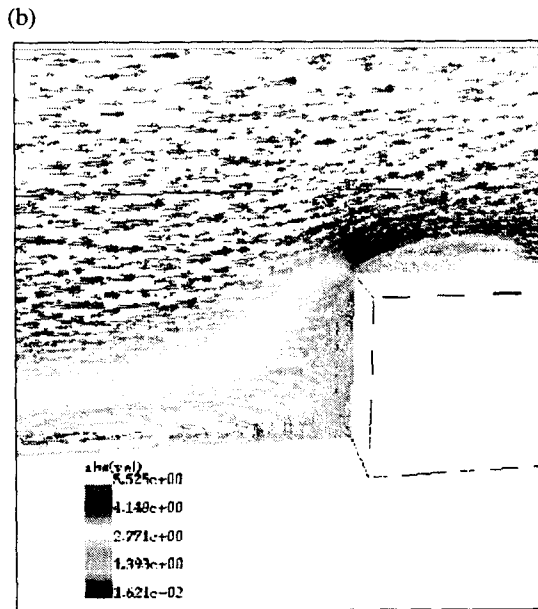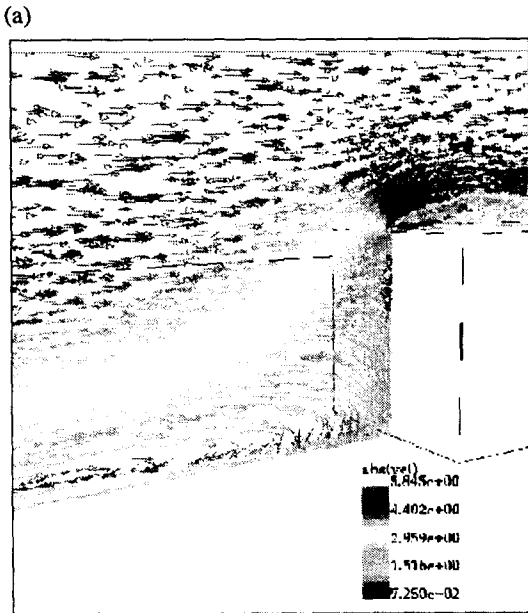
(a)

(b)

Fig. 3. Vector plot for (a) Case 1 and (b) Case 2.

(a)

(b)

Fig. 4. Isosurface of 10% concentration for both cases.

respectively. Figures 5 and 6 show a *horseshoe vortex* around the building area in both cases, which has been previously described in the Hosker review of 1980[2]. Figure 7 shows the flow which passed over the building in both cases. In case 1, most of the flow on the roof passed over the building, whereas case 2 exhibited a strong turn-around flow.
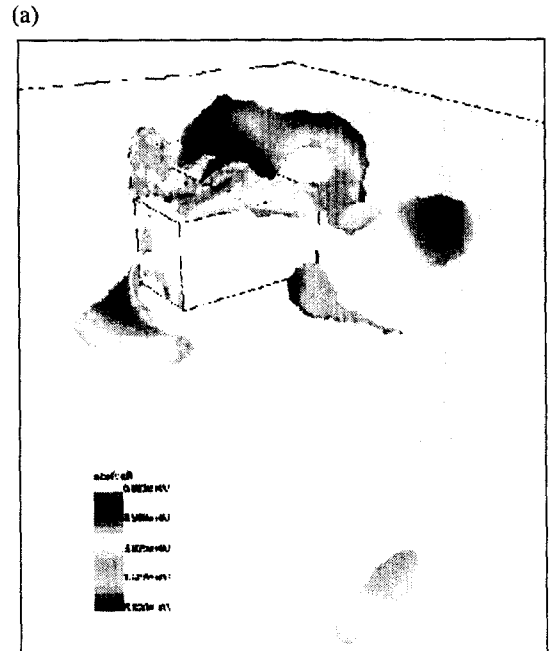
6. Comparison with Wind Tunnel Results

This section compares the numerical results with the data obtained from the wind-tunnel experiment performed in relation to the EMU project[1]. In the
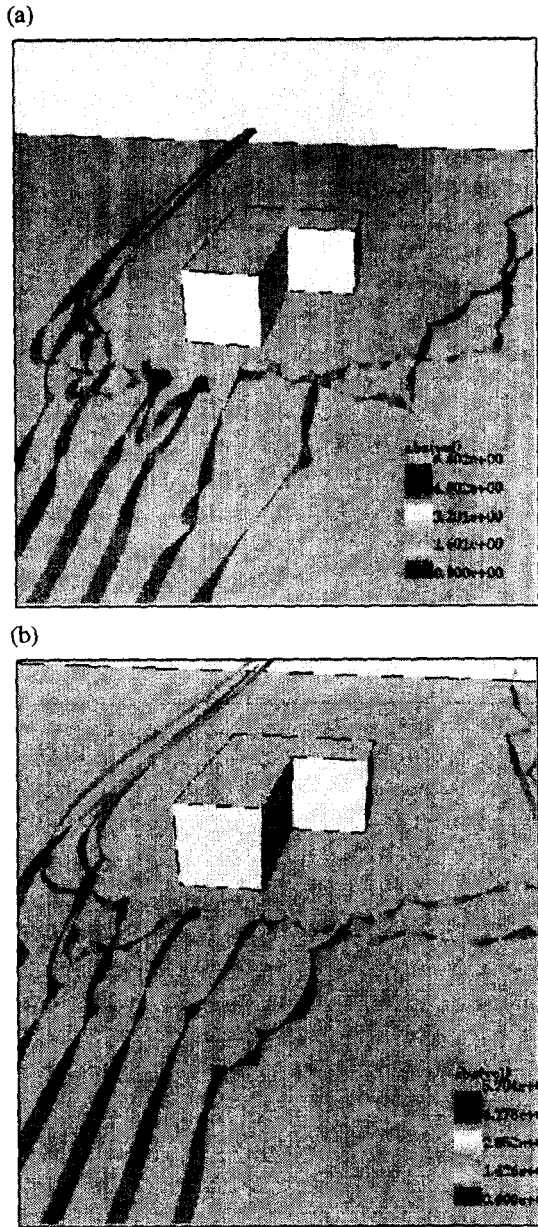
(a)

(b)

Fig. 5. Wind ribbon colored with wind velocity for both cases at 0.2 m from floor.

wind-tunnel experiment, the concentration was normalized to gain a non-dimensional value called C^*. Accordingly, in this study the same process of normalization was performed using the values provided in[1]:

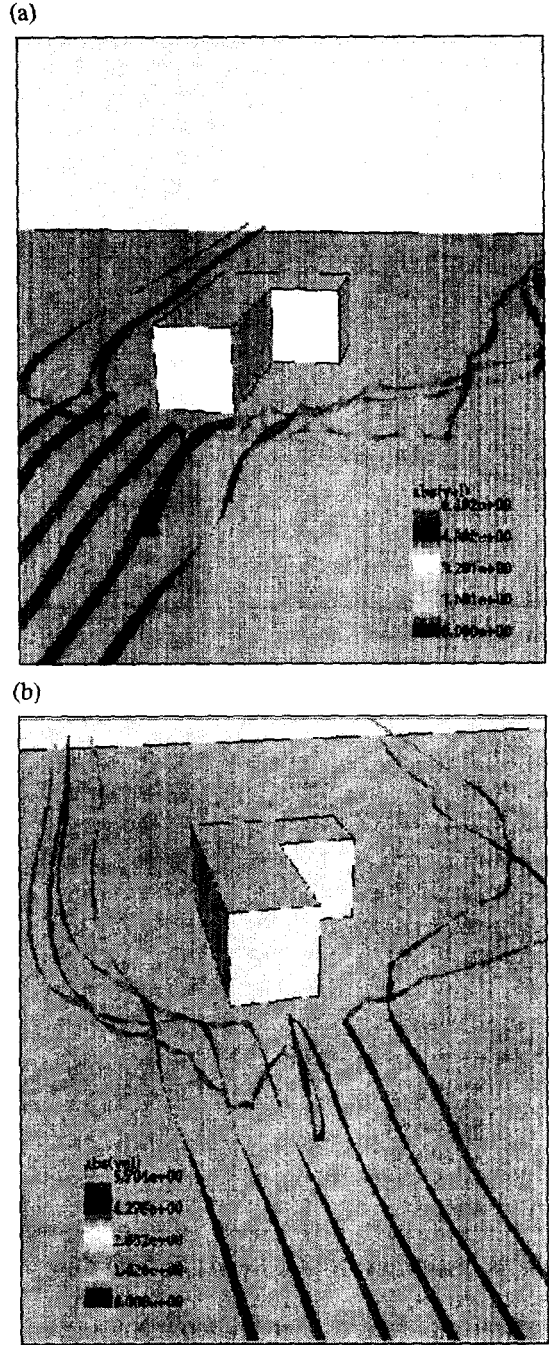$$C^* = \frac{c\ U_h H^2}{Q}, \qquad (11)$$

(a)

(b)

Fig. 6. Same as Fig. 5 except at 5 m from floor.

where c is the concentration, U_h is the average velocity at the height of the building roof, H is the height of the building(10 m) and Q is the source emission rate($Q=20 m^3 s^{-1}$).
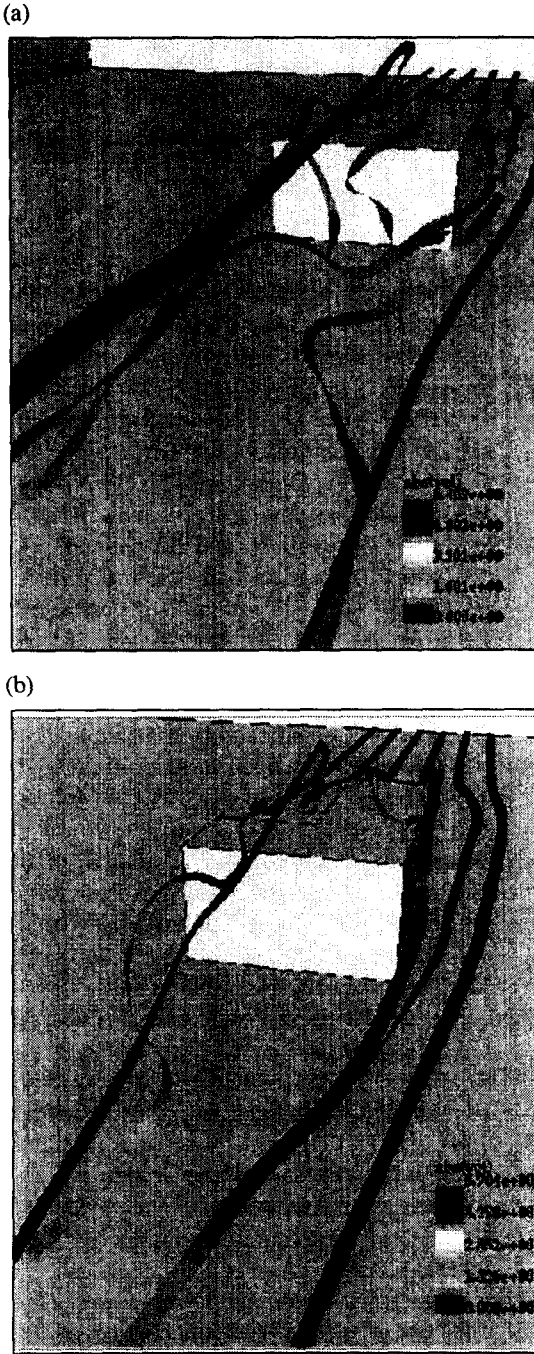
(a)

(b)

Fig. 7. Same as Fig. 5 except at 8 m from floor.

Figure 8 shows the horizontal distribution of the mean concentration at the height of 10 m (z=H), where x is parallel to the inflow direction(see

Fig.1b) and the direction of y is normal to the x-axis. The solid line indicates the wind-tunnel data, whereas the circle and rectangle represent case 1 and 2, respectively. Figure 9 is the same as Fig. 8 except for the vertical distribution of the mean concentration at 100m away from the source. It is clear that case 2 presents a better agreement with the wind-tunnel data than case 1. Accordingly, this indicates that the viscous fluxes closed by $k-\varepsilon$ play an important role when simulating dispersion around a building or obstacle such as a small mountain.
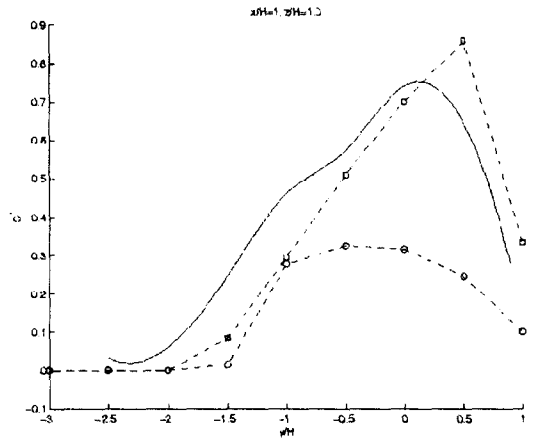

Fig. 8. Comparison between model output and wind-tunnel data with horizontal distribution of mean concentration.
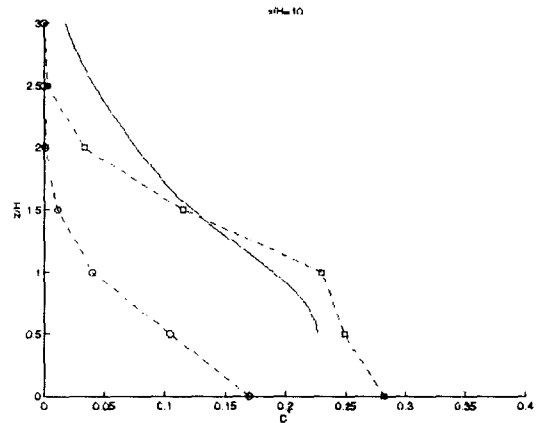

Fig. 9. Same as Fig.8, except for vertical distribution of mean concentration.

7. Conclusions and Outlook

The study of problems on an small scale, like a city or a group of buildings, is still a very difficult topic[14]. Therefore, the combination of previous experimental research in the field with CFD techniques can produce important results. The sample test performed in this study using CFD was successful from the perspective that the code was used as a black box to solve the problem and the results were in agreement with the experimental data available. However, there are still many areas where further study is required to get better results. Since the results using Euler equations and the turbulent model were pretty similar, this would seem to suggest that in this case the geometry of the inflow wind drives the results for the macro scale. It was also noticed that the boundary layer profile in the incoming flow had a very strong influence on the results. Therefore, aspects such as temperature and buoyancy should be also be included in the ensuing steps to have a complete idea of the problem. Another point that needs to be considered is the ability to see all the features mention by Hosker[2] in the flow profile on the upwind and downwind face of the building.

This study presented some results from a release in neutrally stable atmospheric conditions. It was also demonstrated that the results were significantly dependent on the mesh design details, the spatial discretisation scheme, and the turbulence model. This conclusion is not surprising but rather emphasizes the need for great care in undertaking such dispersion simulations with a CFD code.

Other factors, which due to space constraints have not been discussed, can also have non-negligible effects, for example, surface boundary condition details, inlet turbulence profiles, and the domain size or particular type of mesh used(e.g. orthogonal or non-orthogonal). For some applications a factor of two in the predictive variability(or accuracy) of the concentration values may be considered quite adequate, however, this is equally a reason to apply caution to the modelling approach used. For example, the location of the maximum concentration(or dose) may be more important, plus in many circumstances a greater certainty is required for risk or hazard analyses.

Acknowledgements

References

[1] Evaluation of Modelling Uncertainty, CFD Modelling of Near-Field Atmospheric dispersion. Project EMU final report, 1997.

[2] Hosker R. P., "Flow and Diffusion Near Obstacles", in: D. Raderson(Ed.), Atmospheric Science and Power Production. US Dept of Energy, DOE/CR-2521(US Nuclear Regulatory Commission).

[3] Sini J. F., Anquetin S. and Mestayer P. G., "Pollutant Dispersion and Thermal Effects in Urban street Canyons", Atmospheric Environment, Vol. 30, No. 15, pp. 2659~2677, 1995.

[4] Cowan I. R., Castro I. P. and Robins A. G., "Numerical Considerations for Simulations of Flow and Dispersion around Buildings", J. WInd Eng. Ind. Aerodyn., Vol. 67-68, pp. 535~545, 1997.

[5] Dawson P., Stock D. E. and Lamb B., "The Numerical Simulation of Airflow and Dispersion in Three-Dimensional Atmospheric Recirculation Zones", J. Appl. Meteor., Vol. 30, pp. 1005~1024, 1991.

[6] Lohner R., "Recent Progress in Tetrahedral Grid Generation via the Advancing Front Technique", 3rd. International Meshing Roundtable}, Albuquerque, NM, October 1994.

[7] Lohner R., "Extending the Range of Applicability and Automation of the Advancing Front Grid Generation Technique", AIAA 96-0033, 1996.

[8] Lohner R., "Automatic Unstructured Grid Generators", Finite Elements in Analysis and Design. Vol. 25, pp.111~134, 1997.

[9] Lohner R., "Generation of Unstructured Grids Suitable for RANS Calculations", AIAA 99-0662, 1999.

[10] Lohner R., Morgan K., Peraire J. and Vahdati M., "Finite Element Flux-Corrected Trans-

port(FEM-FCT) for Euler and Navier-Stokes Equations", Int. J. Num. Meth. Fluids, Vol. 7, pp.1093~1109, 1987.

[11] Cebral J. R., "ZFEM: Collaborative Visualization for Parallel Multi- disciplinary Applications", Proceedings of Parallel CFD'97, Manchester, U.K., May 19~21, 1997.

[12] Cebral J. R., Lohnerd R., "Interactive On-Line Visualization and Collaboration for Parallel Unstructured Multidisciplinary Applications", AIAA 98-0077, 1998.

[13] Cebral J. R., Lohnerd R., "Advances in Visualization: Distribution and Collaboration", AIAA 99-0693, 1999.

[14] Mestayer P. G., Anquetin S., "Climatology of Cities", in: A.Gyr, F.Rys(Ed.), Diffusion and Transport of Pollutants in Atmospheric Mesoscale Flow Fileds, pp.165~189, 1995.